Solar Phys (2014) 289:153–166
DOI 10.1007/s11207-013-0329-1

A Change in the Solar He II EUV Global Network Structure as an Indicator of the Geo-Effectiveness of Solar Minima

L. Didkovsky · J.B. Gurman

Received: 7 February 2013 / Accepted: 10 May 2013 / Published online: 5 June 2013

Abstract Solar activity during 2007 – 2009 was very low, causing anomalously low thermospheric density. A comparison of solar extreme ultraviolet (EUV) irradiance in the He II spectral band (26 to 34 nm) from the *Solar Extreme ultraviolet Monitor* (SEM), one of instruments on the *Charge Element and Isotope Analysis System* (CELIAS) on board the *Solar and Heliospheric Observatory* (SOHO) for the two latest solar minima showed a decrease of the absolute irradiance of about 15 ± 6 % during the solar minimum between Cycles 23 and 24 compared with the Cycle 22/23 minimum when a yearly running-mean filter was used. We found that some local, shorter-term minima including those with the same absolute EUV flux in the SEM spectral band show a higher concentration of spatial power in the global network structure from the 30.4 nm SOHO/*Extreme ultraviolet Imaging Telescope* (EIT) images for the local minimum of 1996 compared with the minima of 2008 – 2011. We interpret this higher concentration of spatial power in the transition region's global network structure as a larger number of larger-area features on the solar disk. These changes in the global network structure during solar minima may characterize, in part, the geo-effectiveness of the solar He II EUV irradiance in addition to the estimations based on its absolute levels.

Keywords Solar extreme ultraviolet irradiance · Solar cycle · Solar minimum

1. Introduction

The absolute solar EUV irradiance in the He II spectral band of 26 to 34 nm from the *Solar Extreme ultraviolet Monitor* (SEM) was 15 ± 6 % lower during the Cycle 23/24 solar minimum compared with the Cycle 22/23 minimum (Didkovsky *et al.*, 2010). This measured

L. Didkovsky (✉)
Space Sciences Center, University of Southern California, Los Angeles, USA
e-mail: leonid@usc.edu

J.B. Gurman
NASA Goddard Space Flight Center, Greenbelt, MD 20771, USA
e-mail: Joseph.B.Gurman@nasa.gov

lower EUV irradiance combined with the modeled effects, *e.g.* due to the amount of CO_2 in the Earth's atmosphere (Roble and Dickinson, 1989; Qian *et al.*, 2006), caused anomalously low thermospheric density during the most recent solar minimum (Solomon *et al.*, 2010). A number of other investigations showed a global change in the upper atmosphere during the Cycle 23/24 solar minimum (Lastovicka *et al.*, 2006, 2008) including the thermosphere (Emmert *et al.*, 2004; Emmert, Lean, and Picone, 2010), *e.g.* using satellite-drag data (Emmert, Picone, and Meier, 2008). The decrease in the solar irradiance was detected in different spectral bands; see, *e.g.*, the long-term trend in the total solar irradiance (Fröhlich, 2009) or the low solar EUV irradiance in 2008 (Chamberlin *et al.*, 2009). Solomon *et al.* (2011) found that the thermospheric density showed the lowest values at any time in the past 47 years. Both the NCAR Thermosphere–Ionosphere–Electrodynamics General Circulation Model (Roble, Ridley, and Richmond, 1988) and SEM EUV data (Didkovsky *et al.*, 2010) showed good agreement between thermospheric density changes from 1996 to 2008 and the changes in the solar 26 to 34 nm EUV irradiance. Woods (2010) found that the 2008-to-1996 modeled decrease in the XUV (0 to 15 nm) irradiance ratio was even higher, up to 35 %. It remains unclear, however, whether some other change on the Sun is responsible for this significant decrease in the solar irradiance, *e.g.* in the EUV. For example, the oppositely directed effects of the decreased number of polar coronal holes in 2007 (Kirk *et al.*, 2009) and the presence of some large-area, low-latitude coronal holes in 2008 discussed by Woods (2010) make it impossible to conclude whether coronal holes can explain the long-term decrease of solar EUV irradiance during the 2007 – 2009 minimum. Another question is connected to the geo-effectiveness of the absolute solar EUV irradiance during the periods of the same levels of the daily averaged SEM irradiance, *e.g.* in 1996 and 2010: is the geo-effectiveness of the EUV irradiance the same? For example, Solomon *et al.* (2011) mentioned that geomagnetic activity became extremely low in mid-2008 and remained low until late 2009, spanning about 1.5 years of some of the quietest solar–terrestrial conditions ever observed. The authors found that 2009, with an annual average $\mathrm{Ap} = 4$, was slightly lower in annual average density than 2008, although the solar-irradiance conditions were apparently similar.

McIntosh *et al.* (2011a) used a "watershed segmentation" applied to a 30.4 nm image from the EIT (Delaboudinière *et al.*, 1995) to determine the distribution of cell radii in the central portion of the image, up to 0.6 of the solar radius. The segment radii have quite a wide range: about 11 to 40 Mm with the highest frequency of appearance about ten for 24 Mm cells from the 10 April 2008 EIT image. McIntosh *et al.* (2011b) used this method to calculate and compare the mean transition region (TR) network scale for the available EIT 30.4 nm images from 1996 to 2011; see, *e.g.*, the lower panel on Figure 1 of McIntosh *et al.* (2011b). The authors found a significant decrease in the network scale during the Cycle 23/24 solar minimum compared with the Cycle 22/23 minimum.

In this work we analyze spatial power spectra from SOHO/EIT 30.4 nm images for different periods of low solar activity including those for the Cycle 22/23 and Cycle 23/24 solar minima. Instead of using histograms of the cell radii (McIntosh *et al.*, 2011a) or the mean TR network scale (McIntosh *et al.*, 2011b), we compare the spatial power of the images in the whole ranges of the image radii and spatial frequencies. In addition to the method of Magnetic Range of Influence (MRoI: McIntosh, Davey, and Hassler, 2006; Leamon and McIntosh, 2009), this proposed approach may be used to explore how the change in the spatial scale of the TR network affects the Earth's thermosphere.

2. Data Observations

Our analysis of periods of low solar activity is based on EUV images obtained with EIT in the He II band. Data selected for this analysis (Table 1) represent the deepest local solar minima detected in the He II band (last column) by SOHO/CELIAS/SEM during last two Solar Cycles, 22/23 and 23/24, three local minima in 2010 detected by SEM and *Extreme Ultraviolet Spectrophotometer* (ESP: Didkovsky *et al.*, 2012) onboard the *Solar Dynamics Observatory Extreme ultraviolet Variability Experiment* (SDO/EVE: Woods *et al.*, 2012), and one local minimum in 2011. In addition to the EIT images, we also examined spatial power spectra in the 30.4 nm band from the *Atmospheric Imaging Assembly* (AIA: Lemen *et al.*, 2012) on board SDO for comparison of the minima of 2010 and 2011.

Table 1 shows a steady decrease of the sum of the on-disk pixel signals (third column) and the mean level of these signals (fourth column) compared with the changes of the daily averaged absolute 26 – 34 nm SEM flux (last column). This decrease may indicate a degradation of the EIT thin-film aluminum filter. We discuss this and the other forms of degradation in Sections 3 – 5. The numbers in the third and fourth columns are corrected for changes in EIT CCD pixel quantum efficiency [QE] based on the visible-light calibration lamp (CL) tests.

3. Data Reduction

Raw EUV 30.4 nm counts from the original EIT files (Table 1) were first converted to effective data numbers [DN] by subtracting corresponding dark images,

$$C_{\text{eff}}(i, j) = C(i, j) - C_{\text{dark}}(i, j), \tag{1}$$

where i and j are the indices of the image array. The center of the solar disk and its radius from each image file header were used to determine the image pixels outside the disk area and set these pixel signals to zero. As an example, Figure 1 shows an EIT He II solar-disk image for 27 April 1996 in units of DN. Note, all pixel signals outside the disk are set to zero. Then non-zero pixels were organized as an one-dimensional vector

$$C_{\text{eff}}(k) = C_{\text{eff}}(i, j) \tag{2}$$

for the k pixels within the disk area. Bright one-pixel spikes related to the CCD impacts from high-energy particles were replaced with the mean DN for the images. Our goal was to calculate the ratios of the signal distribution as a function of the spatial frequency in the power spectra of these one-dimensional sequences for different groups of files (dates) in Table 1 taken at low levels of solar activity.

3.1. Pixel Degradation and Power Spectra

EIT data files available from umbra.nascom.nasa.gov/eit/eit-catalog are not corrected for degradation. A comparison of the sum of the pixel effective counts (third column in Table 1) for about the same levels of daily averaged SEM absolute flux (last column in Table 1) in April 1996 and August 2010 shows a decrease of roughly a factor of seven. This change of the total solar-disk image brightness is associated with the degradation of the thin-film aluminum filter and/or EIT reflective optics. Similar degradation of the thin-film aluminum filter was determined for the ESP channels based on the daily and weakly calibrations. This degradation of the whole brightness, *e.g.* the mean level, may be easily corrected for by a

Table 1 EIT images selected for periods of low solar activity including some local minima for solar Cycles 22/23 (April and May 1996) and 23/24 (November 2008). Image properties are compared using the sum of on-disk signal in the units of Data Numbers [DN] and the mean disk signal (third and fourth columns). Daily averaged absolute EUV SEM flux in the 26 – 34 nm bandpass is shown in the last column for reference.

Date	File name efz*	Sum of C_{eff}, 10^8 [DN]	Mean signal [DN]	SEM flux, 10^{10} [ph cm^{-2} sec^{-1}]
27 Apr 96	19960427.033225	3.99	380.8	1.08
27 Apr 96	19960427.092959	3.91	373.3	1.08
28 Apr 96	19960428.003126	3.93	376.5	1.08
28 Apr 96	19960428.062000	3.93	374.5	1.09
28 Apr 96	19960428.120829	3.91	372.9	1.09
28 Apr 96	19960428.175716	3.91	373.2	1.09
04 Jun 96	19960604.192903	1.62	309.5	1.17
04 Jun 96	19960604.201208	1.60	305.8	1.17
05 Jun 96	19960605.170704	1.58	301.9	1.18
08 Jun 96	19960608.025934	1.53	291.0	1.19
27 Nov 08	20081127.011936	0.65	123.9	0.95
27 Nov 08	20081127.071936	0.65	124.2	0.95
27 Nov 08	20081127.191936	0.65	124.4	0.95
28 Nov 08	20081128.011935	0.65	123.5	0.94
28 Nov 08	20081128.121937	0.65	123.1	0.94
28 Nov 08	20081128.191937	0.65	123.4	0.94
29 Nov 08	20081129.011934	0.64	121.1	0.93
29 Nov 08	20081129.071936	0.64	121.5	0.93
29 Nov 08	20081129.121938	0.63	121.0	0.93
29 Nov 08	20081129.201937	0.64	122.2	0.93
14 May 10	20100514.011937	0.57	107.8	1.01
14 May 10	20100514.071938	0.58	111.3	1.01
14 May 10	20100514.131938	0.57	108.0	1.01
14 May 10	20100514.191938	0.56	107.6	1.01
15 May 10	20100515.071939	0.56	107.5	1.01
15 May 10	20100515.191938	0.56	106.4	1.01
16 May 10	20100516.011939	0.56	106.1	1.00
16 May 10	20100516.071938	0.56	105.9	1.00
16 May 10	20100516.131938	0.56	106.5	1.00
16 May 10	20100516.191938	0.56	106.0	1.00
26 Aug 10	20100826.011940	0.57	108.2	1.09
26 Aug 10	20100826.131938	0.56	106.8	1.09
27 Aug 10	20100827.011941	0.56	107.0	1.09
28 Aug 10	20100828.131939	0.55	105.3	1.08
19 Dec 10	20101219.011938	0.53	101.8	1.16
20 Dec 10	20101220.012011	0.54	102.2	1.14
20 Dec 10	20101220.131940	0.53	101.4	1.14
21 Dec 10	20101221.011939	0.53	101.2	1.13
21 Dec 10	20101221.131938	0.54	102.2	1.13
22 Dec 10	20101222.011941	0.54	102.2	1.14

Table 1 (*Continued.*)

Date	File name efz*	Sum of C_{eff}, 10^8 [DN]	Mean signal [DN]	SEM flux, 10^{10} [ph cm^{-2} sec^{-1}]
23 Dec 10	20101223.011938	0.53	101.1	1.15
23 Dec 10	20101223.131937	0.53	101.1	1.15
24 Dec 10	20101224.011938	0.53	100.7	1.14
24 Dec 10	20101224.131938	0.52	99.1	1.14
25 Dec 10	20101225.011941	0.51	98.1	1.13
25 Dec 10	20101225.131939	0.51	97.8	1.13
19 May 11	20110519.131941	0.43	82.6	1.28
20 May 11	20110520.011940	0.43	82.7	1.26
21 May 11	20110521.131941	0.43	82.1	1.26
24 May 11	20110524.131620	0.44	83.3	1.27

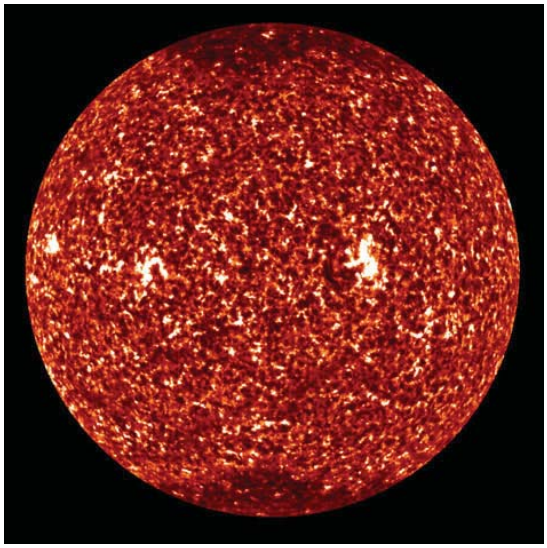

Figure 1 An example of the image reduced according to Equation (1) for 27 April 1996 shows effective counts [C_{eff}] inside the solar disk using a color scale and zero counts outside the disk.

single degradation coefficient [$D(\lambda, t)$] that balances the fluxes for different time intervals. The mean level mean [$C_{\text{eff}}(k)$] is subtracted

$$C_k = C_{\text{eff}}(k) - \text{mean}\big(C_{\text{eff}}(k)\big) \tag{3}$$

in the data prepared for calculating the power spectra [Ψ_f].

$$\Psi_f = \sum_{k=0}^{K-1} C_k \mathrm{e}^{-\mathrm{i}2\pi f k/K}, \tag{4}$$

where $f = 0, \ldots, K-1$ is the spatial frequency array, K is the number of pixels within the solar disk image stored as one-dimensional vector (Equation (2)), and C_k represents either absolute signal variations (Equation (3)) or relative variations

$$C_k = \frac{C_{\text{eff}}(k) - \text{mean}(C_{\text{eff}}(k))}{\text{mean}(C_{\text{eff}}(k))}. \tag{5}$$

Usually, the degradation-related coefficient [$D(\lambda, t)$] is a function of wavelength [λ] and the time [t] of exposure of the filter/optics to solar radiation. For our analysis of the solar

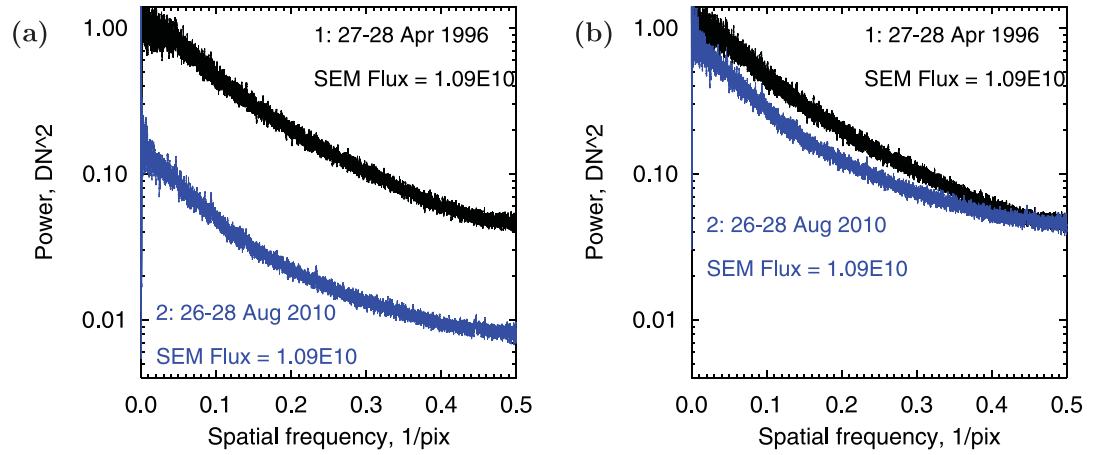

Figure 2 Running-mean curves through the power-spectra data for six files in April 1996 marked as 1 and for four files in August 2010 marked as 2 (see also Table 1). Note the small differences between the curves for each time interval. (a) The curves for 2010 show a lower spectral density due to the throughput degradation $D(1996/2010)$ of the 2010 images compared with the reference images for 1996. For the examples shown in (a) and (b), the spectra were calculated based on the absolute amplitudes (Equation (3)). (b) Same as in (a), but with the levels of the two spectra matching each other for the initial highest spatial frequency by multiplying the spectra for 2010 by $D(1996/2010) = 5.6$. The coefficient $D(1996/2010)$, used to match the curves for the initial frequency, represents a small portion (10^3 points) of the power-spectra data l and thus is different from a degradation ratio based on the sum of the pixel signals or the mean number (third and fourth columns in Table 1).

EIT images in the same 30.4 nm spectral band, the wavelength does not affect the ratios analyzed and the degradation coefficient $[D(t)]$ is a function of time only. This coefficient is the same to correct the degradation of effective counts or the power spectrum based on these effective counts

$$C_1(k)/\big(C_2(k)D(t)\big) = \Psi_1/\big(\Psi_2 D(t)\big), \tag{6}$$

because $D(t)$ is not a function of the pixel number $[k]$. Thus, the power spectrum of the degraded data with decreased levels of the spectral density would be shifted up to match the level of the less degraded curve for the highest spatial frequency. This shift of the whole spectrum brings the ratios between these curves to unity for the highest spatial frequency, which provides a convenient approach to comparing ratios for different spatial frequencies and different temporal intervals. The effect of the degradation is shown in Figure 2(a), where the whole bottom curve for August 2010 represents some spatial power lower than the upper curve for April 1996. Figure 2(b) shows the same curves after the bottom curve was shifted up to match the top curve in Figure 2(a) for the highest spatial frequencies. The multiplicative coefficient $D(1996/2010)$ was determined based on the ratio of the mean power for 10^3 points of the power spectra in the range of frequencies

$$\Delta f = f(K/2) - f(K/2 - 1000). \tag{7}$$

Another degradation factor that we analyzed is related to a possible change of the QE of the EIT CCD pixels as a function of time between detector bake-outs. EIT test data umbra.nascom.nasa.gov/eit/eit_guide/euv_degradation show some changes of pixel QE ratios. These changes were determined using flat-field measurements provided by a visible-light CL. The CL data used in our analysis are shown in Table 2. CCD QE changes based on the CL files (Table 2) were calculated as pixel ratios for each pair of CL images that corresponds to the timing of the group of files used for the comparison (Table 1). The CL

Table 2 EIT calibration-lamp images used to determine the CCD pixel changes of the QE. The images were selected to provide the closest time intervals to the data shown in Table 1

Date	File name efz*
23 May 1996	19960523.153137
24 Jun 1996	19960624.204011
26 Jul 2008	20080726.040008
29 Nov 2008	20081129.040610
15 May 2010	20100515.040053
28 Aug 2010	20100828.040849
18 Dec 2010	20101218.040902
20 May 2011	20110520.040645

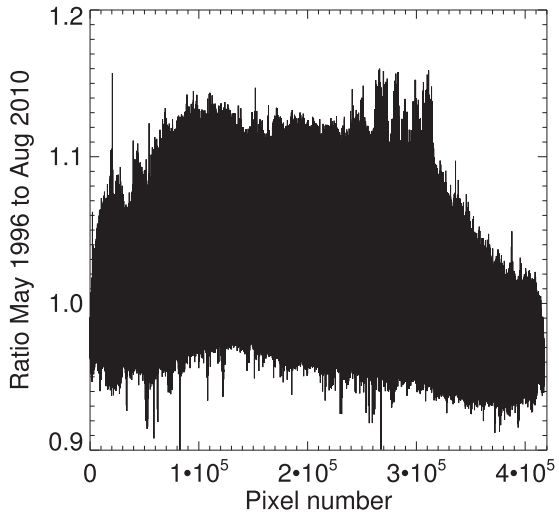

Figure 3 CL pixel ratios for the pixels within the solar-disk area organized as a one-dimensional vector for the images taken on 23 May 1996 and 28 August 2010 (Table 2).

image data were first converted to the effective signals [CL minus dark] and then transferred to one-dimensional arrays for the pixels from the inside of the disk areas, as shown in Equation (2). These ratios $CL_1(k)/CL_2(k)$ were then used to correct the pixel signals

$$C_{\text{corr}}(k) = C_2(k)\frac{CL_1(k)}{CL_2(k)}, \tag{8}$$

where indices 1 and 2 correspond to the earlier and later file dates. As an example, Figure 3 shows the ratios for two CL dates: 23 May 1996 and 28 August 2010.

In addition to the QE changes registered with the visible-light CL, we analyzed whether changes in the power-spectra ratios (next section) might be due to the CCD QE changes in the 30.4 nm EIT spectral band. A wavelength-dependent degradation of the telescope optics, thin-film filters, and CCD could produce degradation similar to that detected by EVE and AIA during the SDO mission. For example, degradation of the thin-film filters decreases the output signals due to the deposition of some hydrocarbons on the filter area. The amount of this deposition is a function of the filter exposure time to the solar radiation and is wavelength dependent.

4. Comparison of Power Spectra for Different Time Intervals with Quiet-Sun Conditions

Power spectra (Equation (4)) were calculated using a one-dimension pixel array that contains relative signal variations (Equation (5)) after their correction for the visible-light CL ratios. For each power spectrum for the solar images (Table 1), a "running-mean" over the spectrum amplitude $[\Psi_f]$ (Equation (4)) was calculated. This low-pass filter is based on the IDL procedure median, which is similar to smoothing with a boxcar or average filter but does not blur edges larger than the neighborhood, with the same integration window of 355 data (spatial frequency) points. The total number of frequency points $[f]$ in the spatial frequency range from zero to 0.5 pix^{-1} for the EIT spectra is about 2^{19}. The number of pixels $[k]$ within the solar-disk area is slightly smaller and the remaining data-array points are filled with its mean number. The 355 data points from the power spectrum used for the integration in the running-mean procedure correspond to a range of spatial frequencies of about 6.8×10^{-4} pix^{-1} for the EIT spectra. These running-mean curves for a number of images within each group of files (Table 1) were averaged and the ratios for each pair of the averaged curves together with the standard deviation (STD) were calculated.

4.1. EIT Power-Spectra Ratios

We have compared power spectra for five different levels of solar activity: four with relatively short time intervals separating them and one with a long time interval. The ratios for short time intervals (Figure 4) are for April 1996 *vs.* June 1996 (diamonds), November 2008 *vs.* May 2010 (filled circles), May 2010 *vs.* August 2010 (squares), and December 2010 *vs.* May 2011 (triangles). Figure 4 shows that the ratios in the spatial frequency range of 0.05 to 0.3 pix^{-1} were highest for the first pair of time intervals (April 1996 *vs.* June 1996) except for the frequency of 0.2 pix^{-1}, and lower for the three later pairs of intervals. This may be interpreted as faster changes of the He II spatial structure of the EIT images in 1996 and about the same small changes in 2008 – 2011.

For the long time interval, we chose two groups of files with about the same level of EUV (30.4 nm) SEM flux of 1.085×10^{10} ph cm^{-2} sec^{-1} for April 1996 and August 2010. The ratios for these time intervals are shown in Figure 5. Figure 5 shows that the ratios between April 1996 and August 2010 power spectra at low spatial frequencies are significant, several times higher than the STD errors.

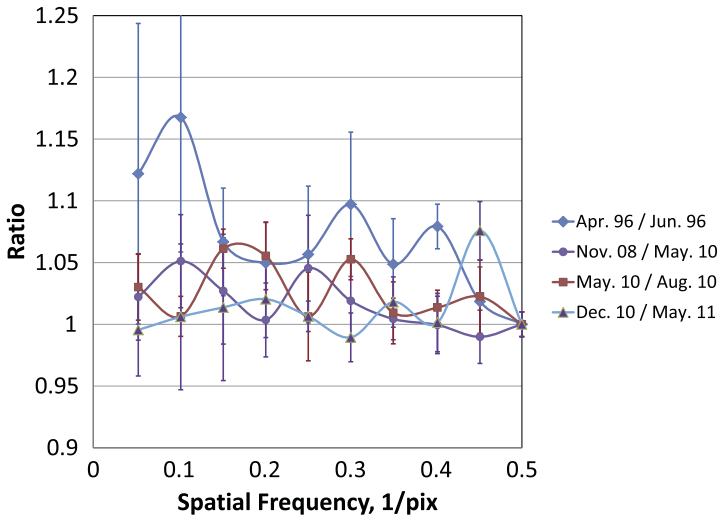

Figure 4 Power-spectra ratios for April 1996 *vs.* June 1996 (diamonds), November 2008 *vs.* May 2010 (filled circles), May 2010 *vs.* August 2010 (squares), and December 2010 *vs.* May 2011 (triangles).

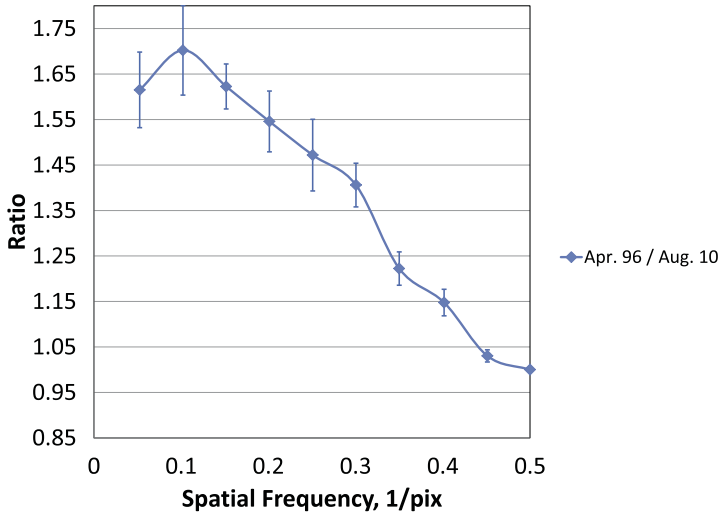

Figure 5 Power-spectra ratios for April 1996 *vs.* August 2010 (diamonds) with about the same level of SEM EUV flux.

Table 3 Averaged ratios and STDs for four pairs of compared time intervals.

Compared time intervals	EIT Ratio	EIT STD	AIA ratio	AIA STD
Apr 1996 *vs.* Jun 1996	1.070	0.05		
Nov 2008 *vs.* May 2010	1.016	0.03		
May 2010 *vs.* Aug 2010	1.035	0.02	1.035	0.01
Dec 2010 *vs.* May 2011	1.031	0.02	1.031	0.02

4.2. Comparison of SOHO/EIT and SDO/AIA Power-Spectra Ratios

Since the beginning of the SDO mission in February 2010, there have been a few time intervals with quiet-Sun conditions. The first two were in May and August 2010. These two time intervals are interesting to compare due to very different operation time and ratios of possible degradation for SOHO/EIT (15 years of observations) and SDO/AIA (less than a year in 2010). Data reduction for the AIA images was similar to that described for EIT images with the difference of the substantially larger size of the one-dimensional array: 2^{23} compared to 2^{19} for EIT and no additional correction for degradation. AIA images were taken from the AIA website www.lmsal.com/get_aia_data/ and SolarSoft IDL programs were used to download the data. For each of the days analyzed, we downloaded six files with a 60-minute cadence. The results of this comparison are shown in Table 3.

5. Discussion

Power spectra for two time intervals in April 1996 and August 2010 (Figure 2(b)) show significant changes of the ratios for the spatial frequencies between 0.05 and 0.4 pix^{-1} (Figure 5). One may think that these ratio differences reflect the degradation of the EIT 30.4 nm channel not corrected by the proposed data reduction. We performed, tested, and compared five "instrumental" approaches to prove that the ratios between the spatial structure of EUV images in 1996 and 2010 are not related to throughput degradation.

The first is a correction of EIT-degraded flux by shifting the data from more recent time intervals to match the spatial frequencies at and below 0.5 pix^{-1} (Figure 2(a) and (b)). This

operation corrects the image degradation related to the decreased reflectivity of the optics and/or decreased transmission of the filters.

The second approach was to compare the ratios for four short time intervals (Figure 4). Figure 4 shows that the ratios for April 1996 *vs.* June 1996 are higher than for the three other pairs of the time intervals. The averaged ratios for these four pairs are shown in the second column of Table 3. If the ratios were related to the degradation, one would expect a steady decrease of the ratios toward the last (10 Dec/11 May) pair. In contrast to this, the ratio for the second pair (filled circles) is lower than for the two last pairs (squares and triangles). Formal STD errors for the averaged ratios are shown in the third column. They show that for all time intervals except for the second, the averaged ratios are higher than unity.

The third test was to compare the ratio results from two EUV 30.4 nm data channels, SOHO/EIT with its 15 years of operation, and SDO/AIA (Table 3) with less than one year of operation in 2010. A comparison of averaged ratios for EIT and AIA (third and fourth rows in Table 3) shows the match of the ratios. This match of the EIT- and AIA-averaged ratios with significantly different time of operation and rate of degradation may be used to prove that the ratios for the third and fourth compared groups reflect the change in the image structures. Table 3 compares the averaged ratios in the whole range of the spatial frequencies that are not affected by the differences in the EIT and AIA spatial resolution: 2.6 and 0.6 [arcsec pix^{-1}] or 1.9 and 0.4 [Mm pix^{-1}].

The fourth test was based on known effects of degradation for the SDO/EVE and SDO/AIA instruments. The degradation reduces the detector/pixel contrast as a function of both exposure time of the instrument to the solar beam and wavelengths. As a result of different EIT and AIA mission (exposure) time, one might expect different ratios for EIT and AIA power spectra (third and fourth rows in Table 3), which is not the case. In addition to the averaged ratio comparison in Table 3, we tested the ratios for the pair shown in Figure 5, but with a number of different contrast coefficients. The pixel-contrast variations for the most recent images (August 2010) used to compare with the April 1996 images (Figure 5) were modified $[C_{\mathrm{mod}}(k)]$ using Equations (9) and (10). Equation (9) was used for a pixel signal stronger than the mean $[C_{\mathrm{mean}}(k)]$ for the one-dimensional array. Equation (10) was used for pixel signals weaker than the mean $[C_{\mathrm{mean}}(k)]$, where

$$C_{\mathrm{mod}}(k) = C(k)m \tag{9}$$

or

$$C_{\mathrm{mod}}(k) = C(k)/m, \tag{10}$$

where m is the contrast increase/decrease coefficient. Figure 6 shows a set of ratio curves for the original ratios (bottom curve) and for the power spectra using modeled images with modified contrast. Figure 6 shows that the changes of the pixel contrast of the most recent images in a wide range of m, from 0.8 to 2.5, do not decrease the ratios compared with the original curve. This test proves that the change of the image pixel-to-pixel contrast associated with the degradation of the August 2010 EIT images compared with the less-degraded April 1996 images does not lead to the smaller spatial differences of the ratios, which could be close to unity for the similar spatial structures.

Finally, a fifth test consisted of adding two realizations of random noise, with a smaller and an order of magnitude larger amplitude to the pixel signals of the August 2010 and April 1996 images. The results of added pixel-to-pixel random noise shows some increase of the spatial power at high spatial frequencies (0.35 to 0.5) pix^{-1}, but does not affect the power (and ratios) at lower spatial frequencies.

These five "instrumental" tests lead us to conclude that the measured ratios based on the power spectra differences for 1996 *vs.* 2010 with about the same EUV SEM flux in the

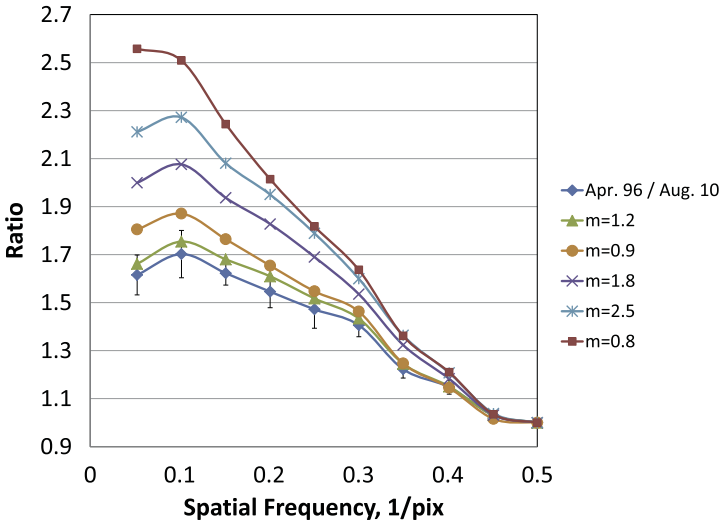

Figure 6 A comparison of power-spectra ratios for the original pair (diamonds) of time intervals April 1996 *vs.* August 2010 and the ratios for five modified contrast curves above it for m equal to 1.2 (triangles), 0.9 (filled circles), 1.8 (crosses), 2.5 (stars), and 0.8 (squares). We modified the contrast of the most recent (more degraded) series of the EIT images.

30.4 nm band (Figure 5) are not related to a component of EIT throughput degradation that has not been accounted for by our data-reduction algorithm.

If the 1996 *vs.* 2010 differences (Figure 5) in the spatial ratios are not due to "instrumental" sources, which solar sources could be responsible? To determine which solar feature(s) is (are) responsible for the changes of the ratios, three tests were performed. First, we compared the ratios from the power spectra with polar regions removed from the solar-disk images to exclude polar coronal holes, visible, *e.g.*, in Figure 1. The result of these modified spectra was practically the same as for the full-Sun images.

Second, we compared the ratios for only the central portions of the solar disk with a limiting radius equal to 0.75 of the original radius. In addition to removing the polar regions from the disk images, this procedure also removes areas close to the limb with image radii between 0.75 and 1.00. The result was the same, with no more than a 3 % change to the ratios.

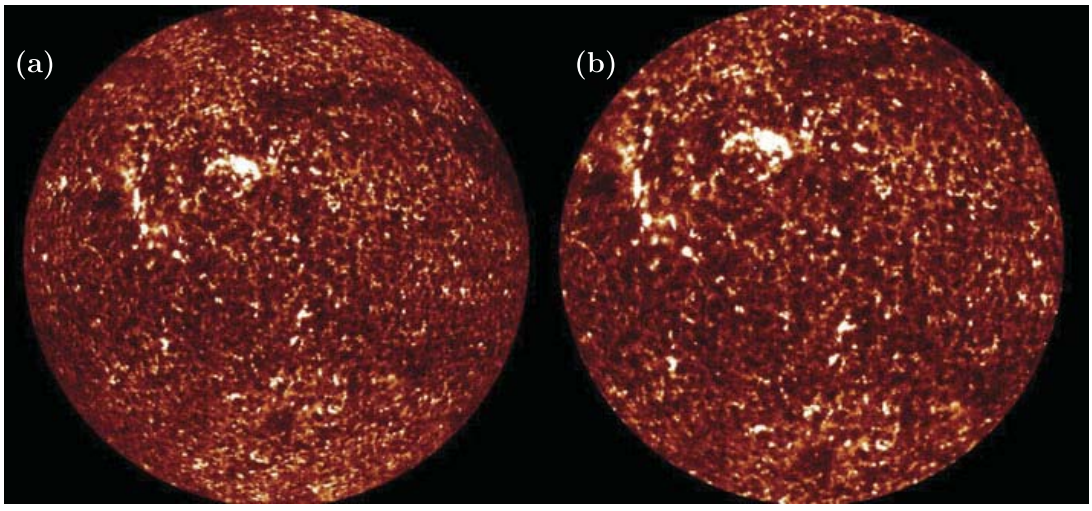

Figure 7 (a) Original EIT 30.4 nm solar image for 28 August 2010 at 13:19:39. (b) The same image, but first stretched from 1024 × 1024 pixels to 1280 × 1280 pixels and then saved with the same format as the left image.

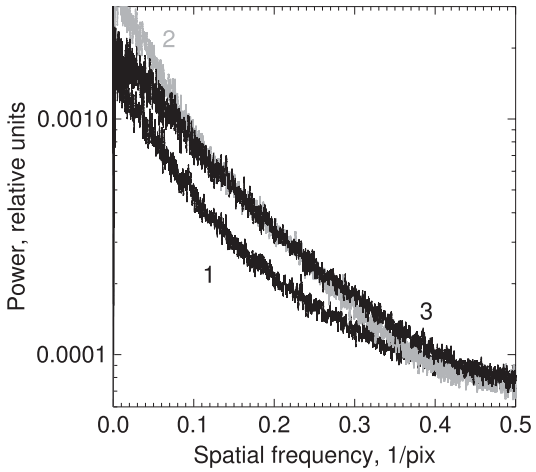

Figure 8 A comparison of power-spectra running-mean curves for the original image (Figure 7(a)), stretched image (Figure 7(b)), and for 27 April 1996 (Figure 1), thin black marked as 1, gray marked as 2, and thick black marked as 3, correspondingly.

Finally, we stretched the solar image for 28 August 2010 at 13:19:39 (Figure 7(a)) to change the spatial dimensions of the solar features on the disk (Figure 7(b)). The stretching procedure is to increase the image size by 1.25 times and then use the same image area as in the original image. The increase of the image dimensions increases the spatial details of the He II structure on the image (compare Figure 7(a) and (b)). Saving the same area on the stretched image causes the removal of a small outer ring compared to the original image. The result of this procedure is shown in Figure 8, which shows that the 25 % stretched image increases the power on the intermediate and low spatial frequencies (compare curves 1 and 2 shown as thin black and gray curves) and leads to about the same power as for the 1996 image (thick black curve marked as 3). A small decrease of the power for the stretched image (gray) at high spatial frequencies, *e.g.* at 0.4 pix^{-1}, is the result of removing the outer ring with its foreshortened features from the stretched image.

6. Results

Our goal was to compare the spatial ratios for two solar minima, between Cycles 22/23 and Cycles 23/24 and for a number of local minima for 2008 – 2011. Figure 9 compares ratios for the Cycle 22/23 *vs.* Cycle 23/24 solar minima and ratios for another pair of quiet-Sun conditions: 1996 *vs.* 2010 with about the same level of SEM EUV flux. Figure 9 shows that the smallest change in the network structure between 1996 and either 2008 or 2010 images occurred for small-area solar features with spatial scales up to three EIT pixels (< 5.7 Mm). For the larger-area features (> 3 EIT pixels or > 5.7 Mm) the ratio curve for 1996 *vs.* 2008 (diamonds) shows lower ratios than the 1996 *vs.* 2010 ratios (squares) with the difference outside the error bars for the spatial frequency of 0.15 pix^{-1} (about six EIT pixels or about 11.3 Mm). This result shows that the images from the local activity minimum of 2010 contained fewer features with a spatial size of three to ten pixels (5.7 to 18.8 Mm) than during the Cycle 23/24 minimum and significantly fewer than during the Cycle 22/23 minimum.

We found small changes in the ratios for the local minima within the current solar cycle, 2008 – 2011 (three bottom curves in Figure 4 and three bottom rows in Table 3). They may indicate a number of returns to the conditions of He II TR network structure derived from the spatial power spectra for the Cycle 23/24 solar minimum with the increased levels of the SEM 30.4 nm solar irradiance, up to 34 % for the minimum of 2011. The ratios for another short time interval (April 1996 *vs.* June 1996) are substantially higher on low- and intermediate-spatial frequencies than between December 2010 and May 2011 (compare curves marked with diamonds and triangles in Figure 4).

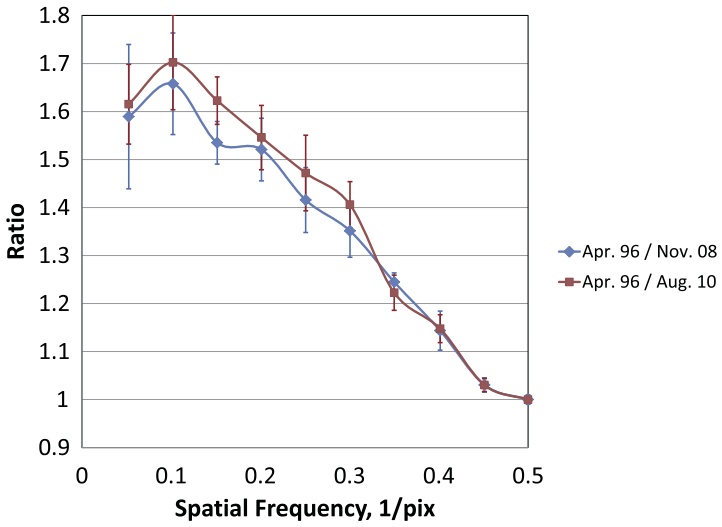

Figure 9 A comparison of power-spectra ratios for the two pairs of time intervals, one (diamonds) to compare the global He II network structure during two solar minima in April 1996 and in November 2008, another (squares) to compare the April 1996 minimum with the May 2010 local minimum with about the same SEM fluxes (Table 1), 0.94 and 1.01 $\times 10^{10}$ [ph cm^{-2} sec^{-1}].

7. Concluding Remarks

We found that for about the same level of EUV 30.4 nm solar flux from the SEM daily averaged fluxes, the ratios for 1996 *vs.* 2010 (see squares in Figure 9) are significantly higher than unity, which appears to be correlated with the change in the distribution of transition-region network structure sizes analyzed for the 2008 – 2011 minima. The change of the network structure is consistent with a decreased population of mid-sized features on the solar disk. The same EUV 30.4 nm daily averaged fluxes for these different structures of the transition-region network may be related to the re-distribution of the coronal holes and the higher intensity (contrast) of the small features for the Cycle 23/24 solar minimum and for the local minima of 2010 and 2011 compared with the Cycle 22/23 minimum. These results show that not only the absolute level of EUV irradiance, but its spatial distribution in the transition region may have to be considered in predicting solar-cycle effects on the thermosphere.

The power spectra and the ratios analyzed in this article show a decrease of the TR spatial He II structure during the prolonged Cycle 23/24 solar minimum. This is consistent with the decrease of the mean TR network scale (McIntosh *et al.*, 2011b) determined using the "watershed segmentation" method (McIntosh *et al.*, 2011a). The spectra show *smooth* increases of the power toward the low spatial frequencies (larger network features). In addition to the results from the "watershed segmentation" method (McIntosh *et al.*, 2011a), which provides histograms with the distribution of the cell radii in the central portion of the image, the spectra contain a combined effect of the sizes of the structures and their spatial spectral density. If spatially resolved measurements of He II emission are maintained through several solar minima, we should be able to conclude whether the spatial distribution of that emission provides a proxy for predicting cycles with anomalously prolonged minima.

Acknowledgements This work was partially supported by the University of Colorado award 153-5979. SOHO is a project of international cooperation between NASA and ESA.

References

Chamberlin, P.C., Woods, T.N., Crotser, D.A., Eparvier, F.G., Hock, R.A., Woodraska, D.L.: 2009, *Geophys. Res. Lett.* **36**, L05102. doi:10.1029/2008/GL037145.

Delaboudinière, J.-P., Artzner, G.E., Brunaud, J., Gabriel, A.H., Hochedez, J.F., Millier, F., Song, X.Y., Au, B., Dere, K.P., Howard, R.A., *et al.*: 1995, *Solar Phys.* **162**, 291. ADS:1995SoPh..162..291D. doi:10.1007/BF00733432.

Didkovsky, L.V., Judge, D.L., Wieman, S.R., McMullin, D.: 2010, In: Cranmer, S.R., Hoeksema, J.T., Kohl, J. (eds.) *SOHO23: Understanding a Peculiar Solar Minimum* **CS-428**, Astron. Soc. Pac., San Francisco, 73.

Didkovsky, L., Judge, D., Wieman, S., Woods, T., Jones, A.: 2012, *Solar Phys.* **275**, 179. ADS:2012SoPh..275..179D. doi:10.1007/s11207-009-9485-8.

Emmert, J.T., Lean, J.L., Picone, J.M.: 2010, *Geophys. Res. Lett.* **37**, L12102. doi:10.1029/2010/GL043671.

Emmert, J.T., Picone, J.M., Meier, R.R.: 2008, *Geophys. Res. Lett.* **35**, L05101. doi:10.1029/2007/GL032809.

Emmert, J.T., Picone, J.M., Lean, J.L., Knowles, S.H.: 2004, *J. Geophys. Res.* **109**, A02301. doi:10.1029/2003JA010176.

Fröhlich, C.: 2009, *Astron. Astrophys.* **501**, L27. doi:10.1051/0004-6361/200912318.

Kirk, M.S., Pesnell, W.D., Young, C.A., Hess Weber, S.A.: 2009, *Solar Phys.* **257**, 99. ADS:2009SoPh..257..99K. doi:10.1007/s11207-009-9369-y.

Lastovicka, J., Akmaev, R.A., Beig, G., Bremer, J., Emmert, J.T.: 2006, *Science* **314**, 1253. doi:10.1126/science.1135134.

Lastovicka, J., Akmaev, R.A., Beig, G., Bremer, J., Emmert, J.T., Jacobi, C., Jarvis, M.J., Nedoluha, G., Portnyagin, Y.I., Ulich, T.: 2008, *Ann. Geophys.* **26**, 1255. doi:10.5194/angeo-26-1255-2008.

Leamon, R.J., McIntosh, S.W.: 2009, *Astrophys. J. Lett.* **697**, L28. doi:10.1088/0004-637X/697/1/L28.

Lemen, J.R., Title, A.M., Akin, D.J., Boerner, P.F., Chou, C., Drake, J.F., Dunkan, D.W., Edwards, C.G., Friedlaender, F.M., Heyman, G.F., *et al.*: 2012, *Solar Phys.* **275**, 17. doi:10.1007/s11207-011-9776-8.

McIntosh, S.W., Davey, A.R., Hassler, D.M.: 2006, *Astrophys. J. Lett.* **644**, L87.

McIntosh, S.W., Leamon, R.J., Hock, R.A., Rast, M.P., Ulrich, R.K.: 2011a, *Astrophys. J. Lett.* **730**, L3. doi:10.1088/2041-8205/730/1/L3.

McIntosh, S.W., Kiefer, K.K., Leamon, R.J., Kasper, J.C., Stevens, M.L.: 2011b, *Astrophys. J. Lett.* **740**, L23. doi:10.1088/2041-8205/740/1/L23.

Qian, L., Roble, R.G., Solomon, S.C., Kane, T.J.: 2006, *Geophys. Res. Lett.* **33**, L23705. doi:10.1029/2006GL027185.

Roble, R.G., Dickinson, R.E.: 1989, *Geophys. Res. Lett.* **16**, 1441. doi:10.1029/GL016i012p01441.

Roble, R.G., Ridley, E.C., Richmond, A.D., Dickinson, R.E.: 1988, *Geophys. Res. Lett.* **15**, 1325. doi:10.1029/GL015i012p01325.

Solomon, S.C., Woods, T.N., Didkovsky, L.V., Emmert, J.T.: 2010, *Geophys. Res. Lett.* **37**, L16103. doi:10.1029/2010GL044468.

Solomon, S.C., Qian, L., Didkovsky, L., Viereck, R., Woods, T.N.: 2011, *J. Geophys. Res.* **116**, A00H07. doi:10.1029/2011JA016508.

Woods, T.N.: 2010, In: Cranmer, S.R., Hoeksema, J.T., Kohl, J. (eds.) *SOHO23: Understanding a Peculiar Solar Minimum* **CS-428**, Astron. Soc. Pac., San Francisco, 63.

Woods, T.N., Eparvier, F.G., Hock, R., Jones, A., Woodraska, D., Judge, D., Didkosky, L., Lean, J., Mariska, J., Warren, H., McMullin, D., Chamberlin, P., Berthiaume, G., Bailey, S., Fuller-Rowell, T., Soika, J., Tobiska, W.K., Viereck, R.: 2012, *Solar Phys.* **275**, 115. ADS:2012SoPh..275..115W. doi:10.1007/s11207-009-9487-6.